1

Properties of ZnO

As an important semiconductor material, zinc oxide (ZnO) has been studied extensively during the past decade due to its many unique properties. In this chapter, the crystal structures of ZnO and its key physical properties such as electrical, optical and piezoelectric properties will be presented in detail.

1.1. Crystal structure of ZnO

ZnO is an inorganic binary compound belonging to the II–VI semiconductor material group. As most of the group II–VI binary compound semiconductors, ZnO crystallizes both in cubic zinc blende and in hexagonal wurtzite structure. As presently known, ZnO possesses three different crystallographic phases: wurtzite (B4), zinc blende (B3) and rocksalt (B1), as schematically shown in Figure 1.1.

The wurtzite structure ZnO (hexagonal) is thermodynamically stable at room temperature. The zinc blende structure ZnO (cubic) is metastable and can be stabilized only by hetero-epitaxial growth on cubic symmetry substrates. The rocksalt structure (cubic, NaCl) can be obtained applying a relatively high pressure (10–15 GPa) to the wurtzite structure; it is a metastable phase but it can persist at atmospheric pressure. Therefore, most used ZnO, natural or synthesized, have the wurtzite structure.

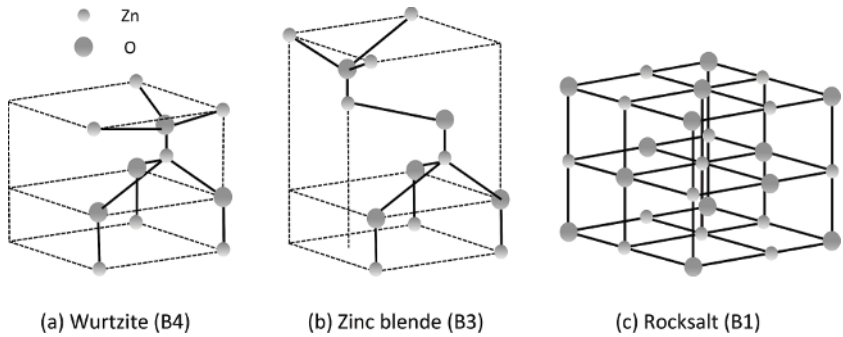

Figure 1.1. *Three crystalline structures of ZnO: a) wurtzite (hexagonal symmetry), b) blende (cubic symmetry) and c) rocksalt (cubic symmetry)*

The wurtzite structure belongs to the space group C_{6v}^4 in the Schoenflies notation and $P6_3mc$ in the Hermann–Mauguin notation. The primitive cell of the wurtzite structure can simply be described by two compact hexagonal networks, one of the Zn^{2+} and the other of the O^{2-}, shifted a vector $\vec{u}$ = 3/8 $\vec{c}$ = 0.375 $\vec{c}$ (in an ideal wurtzite structure), which corresponds to the existing translation between the two subnetworks. In fact, the structure is a tetrahedral stack of $Zn[O]_4$ interpenetrating each other. In an ideal wurtzite structure, the hexagonal unit cell has a ratio of $c/a = \sqrt{8/3} = 1.633$, but the experimentally observed c/a ratios are often smaller than the ideal ratio. The lattice parameters of ZnO wurtzite structure commonly measured at room temperature by X-ray diffraction (XRD) range from 3.2475 to 3.2501 Å for the *a*-parameter and from 5.2042 to 5.2075 Å for the *c*-parameter, with the ratio of $c/a \approx 1.602$ [MOR 09].

The alternating oppositely charged ions plans, positive (0001) -Zn and negative $(000\bar{1})$-O, naturally create a polarity of these surfaces which are closed with non-polar surfaces $(10\bar{1}0)$ and $(11\bar{2}0)$. This structure reveals a polarization along the *c*-axis. This polarization and lack of central symmetry of the wurtzite structure make the ZnO piezoelectric properties exploitable in the field of electricity generators for self-powered devices.

1.2. Electrical properties of ZnO and Schottky junction ZnO/Au

ZnO is a semiconductor with a direct and large bandgap of ~3.37 eV at room temperature; this energy, also called gap, corresponds to the necessary energy to pass an electron from the valence band to the conduction band. ZnO also owns a large exciton binding energy of 60 meV [MUY 57, SER 97]. Theoretically, an undoped ZnO is intrinsically n-type due to the formation of donors such as O vacancies and Zn interstitials [MIN 86]. By doping, we can obtain the gap values of ZnO from 3.30 to 3.39 eV [REB 02, NG 98]. The dopants generally used for ZnO belong to groups III and IV of the periodic table. In this case, they will replace the zinc atoms occupying in their atomic sites. The elements of group VII can also be used as dopants, and in this case the doping takes place by substituting the oxygen atoms in ZnO.

Due to its interesting and versatile properties, ZnO is attracting much attention for many electronic and optoelectronic applications. All applications involving the ZnO nanowire arrays require a reliable Ohmic and/or Schottky electrical connection between the ZnO nanowires and the substrate and/or electrodes (junction ZnO/metal). Therefore, a better understanding of the electrical contact nature between the substrate and/or electrodes and the ZnO is necessary and critical for all devices based on the ZnO nanowire arrays.

There are two types of contact between a metal and a semiconductor: Ohmic and Schottky. The electrical contact between a metal and a semiconductor may be Ohmic when the current–voltage characteristic (*I–V* curve) of the junction is linear; this means that the electrons have a symmetric transport at either forward or reversal bias due to non-existent potential barrier at the metal/semiconductor interface. When a potential barrier is formed at the interface, the electrons across this interface will not be symmetric; thus, the current may be adjusted according to the applied voltage: this type of contact is called Schottky contact in honor of the German physicist Walter H.

Schottky, who demonstrated the theory for the understanding of this phenomenon in 1938 [SCH 38].

In fact, in a metal, the electrons fill all the energy states to the Fermi level E_f. To extract an electron at the Fermi level, it is necessary to provide a work function φ_m (Figure 1.2(a)); while in a semiconductor, the energy required to extract an electron in the conduction band is called the electron affinity χ_s (Figure 1.2(b)). When a metal and a semiconductor are joined, a potential barrier of $\varphi_{sb} = \varphi_m - \chi_s$, called Schottky barrier, will be formed at the interface. According to the φ_m and χ_s values, the contact may be Ohmic if $\varphi_m < \chi_s$, and it may be Schottky if $\varphi_m > \chi_s$. Figure 1.2(c) shows the configuration of metal/n-type semiconductor junctions when they form a Schottky contact. Table 1.1 shows the work function values for some commonly used metals and the contact type with ZnO [HAY 08], knowing that the electron affinity of ZnO is of about 4.5 eV [HAS 05]. It is worth noting that the metal work function depends on its atom configuration at the surface. For example, the work function of the polycrystalline silver is 4.26 eV, but for silver crystals it varies according to crystal faces: 4.64 eV on (100) face, 4.52 eV on (110) face and 4.74 eV on (111) face [DWE 75].

The presence of a Schottky contact at the metal/semiconductor interface acts as a "diode". Under a forward bias, the metal has a higher potential, the electrons near the interface leave the donor states of the semiconductor to go to the metal side, and thus the current can flow through the barrier. On the contrary, under a reversal bias, the metal has a lower potential, so the electrons cannot overcome the barrier to reach the semiconductor side leading a current off state. During the metal/n-type semiconductor junction formation, the electrons leave the interface on the semiconductor side leading a positive space charge region called depletion zone with a length *d* (Figure 1.2(c)). Similarly, a negative charge region forms the metal side of this junction; and at equilibrium, the Fermi levels of the two materials are at an equal level.

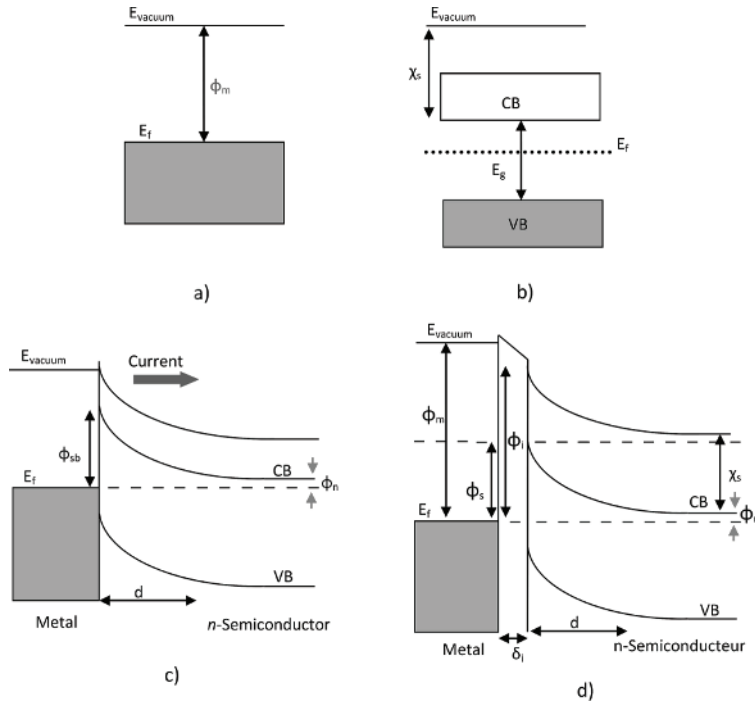

Figure 1.2. *Electronic levels in a metal a) and an n-type semiconductor b). c) Energy diagram of the Schottky junction under forward bias without c) and with d) the interface layer*

Element	*Ag*	*Au*	*Pt*	*Pd*	*Ti*	*Al*	*Si*
Work function (eV)	4.26–4.74	5.1–5.47	5.12–5.93	5.22–5.6	4.33	4.06–4.26	4.60–4.85
Contact type	Ohmic/ Schottky	Schottky	Schottky	Schottky	Ohmic	Ohmic	Schottky

Table 1.1. *Work function of some metals and their contact type with ZnO*

In the case of perfect contact between the metal and the semiconductor, the slope of the relation proposed by Schottky $\phi_{sb} = \phi_m - \chi_s$ should be equal to 1. However, experimental observations demonstrated that this relationship is valuable only for the wide bandgap semiconductor (e.g. $E_g > 4$ eV) [KUR 69]. In fact,

the model proposed by Schottky ignores interface states. Bardeen [BAR 47] introduced the idea of the existence of interface states whose energy would be located within the gap of semiconductor, and which would increase the conductivity at the junction. Therefore, the height of the barrier is influenced by these interface states, which explains the difference between the Schottky model and the experimental observations. The energy diagram in the presence of the interface layer is shown in Figure 1.2(d), where ϕ_i is the interface energy extraction and ϕ_i is the dipole width created by the contact between the metal and the interface layer, which is originated from the difference in energy extraction $\phi_i - \phi_m$.

The Schottky contact between the metal and ZnO is a key factor for the current generation of the ZnO nanowire-based piezoelectric nanogenerator.

Before the determination of the characteristic parameters of the junction ZnO nanowires/metal, it is useful to carry out the measurements on the ZnO thin films allowing a post-comparison. In order to determine the resistivity of the ZnO thin film, two Ohmic contacts (bottom and top) are necessary. Figure 1.3 shows the experimental process for the electrical measurement on the electrodeposited ZnO thin film between two aluminum (Al) contacts [BRO 11]. The top microelectrodes were chosen to perform under same conditions both for ZnO thin film and nanowires: multi-top microelectrodes allow a good repeatability for experimental results. Figures 1.4(a) and (b) show the experimental setup for *I–V* characterization and Figure 1.4(c) shows a typical *I–V* characteristic obtained between one of the microelectrodes and the bottom electrode, from which the electrical resistivity of electrodeposited ZnO thin film can be estimated at about 0.06 ± 0.02 Ω cm. In the literature, we can find the resistivity values between 0.001 and 0.1 Ω cm for ZnO thin film obtained by different synthesis methods [SCH 99, OZG 05]. These values are in agreement with the ZnO bulk value and the lower resistivity is due to the defects in side of the synthesized ZnO micro- and nanostructure ZnO such as the oxygen vacancies and/or interstitial zinc [BAR 47].

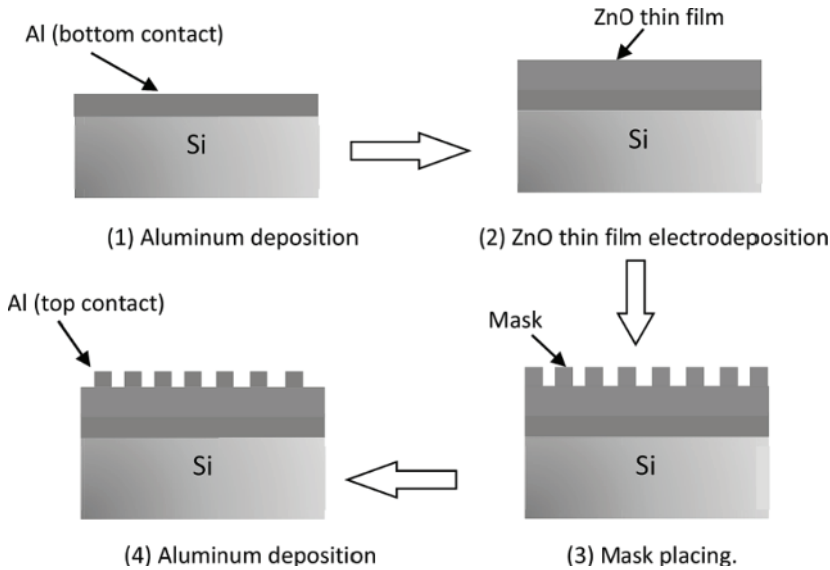

Figure 1.3. *Sample preparation for I–V measurements on electrodeposited ZnO thin film with top and bottom Ohmic contacts*

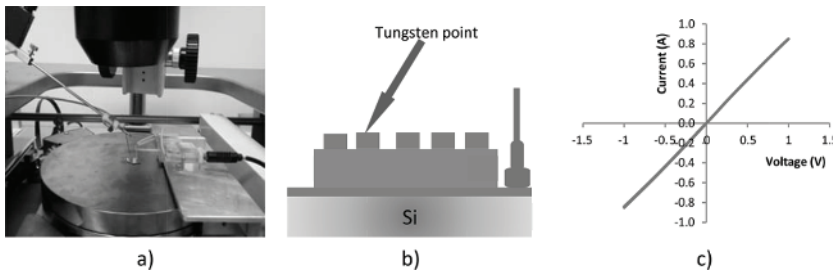

Figure 1.4. *a) and b): experimental setup for I–V measurements used both for ZnO thin film and the nanowires. c): a typical I–V characteristic obtained between one of the microelectrodes and the bottom electrode*

The first step to measure the Schottky junction between ZnO nanowires and the bottom Au contact is the deposition of an Al top Ohmic contact. The quality of the top electrical contact is crucial both

for the transport behavior and the device performance. The fabrication of the top Al electrodes on ZnO nanowire arrays was a challenge regarding the very rough surface and the possible short circuits, so it is impossible to make the metal deposition directly on the nanowire arrays.

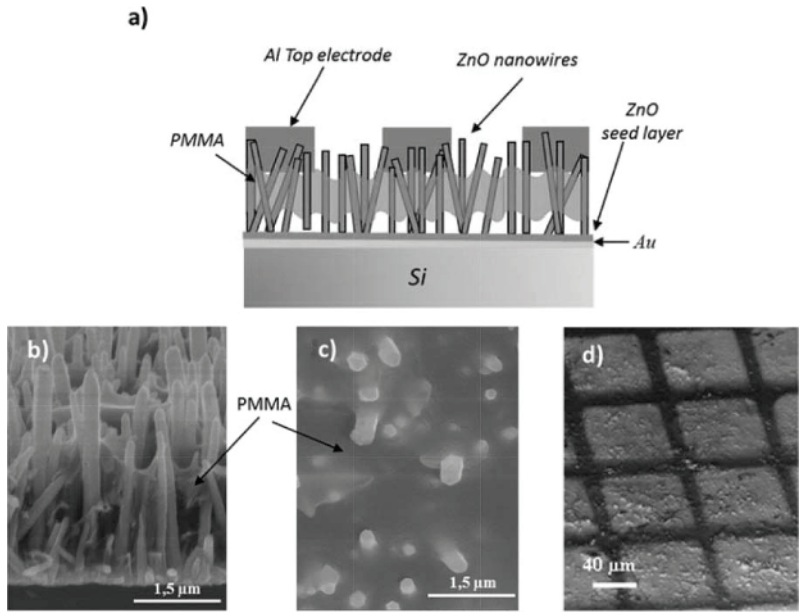

Figure 1.5. *a) Schematic description of electrical contact made on ZnO nanowire arrays: a PMMA layer was spin-coated before Al top electrodes deposition. b) Tilted and c) top-view SEM images of the ZnO nanowire arrays after PMMA layer deposition. d) SEM image of the top aluminum microelectrodes (80 × 80 µm^2) deposited on the ZnO nanowire arrays*

To overcome this difficulty, we adopted a method to make reliable contact on top of the ZnO nanowire arrays, which is schematically shown in Figure 1.5(a): a thin insulator Poly(methyl methacrylate) (PMMA) layer of ~100 nm is firstly spin-coated on the surface of the ZnO nanowires array before metal electrode deposition. The purpose of this PMMA coating is to make a continuous and relatively smooth supporting layer for the metal pad deposition in order to optimize the electric contact with the nanowire arrays; it also plays an important

isolating role between the top Al electrode and the Al/Au bottom electrode to avoid possible short circuit. The scanning electron microscopy (SEM) images shown in Figures 1.5(b) and (c) reveal the detail of the PMMA coating on the ZnO nanowire arrays. After an ultraviolet (UV) treatment of the PMMA, top electrode arrays were sputtered through a shadow mask on the surface of ZnO nanowires. Figure 1.5(d) shows the SEM image of the square-shaped aluminum pads (80 μm in width) on the ZnO, on which we can see that the ZnO nanowire array has been quiet well recovered by an Al layer [BRO 14].

Figures 1.6(a) and (b) show the characteristic *I–V* curves from the asymmetric configuration (Al/ZnO/Au), measured both on the electrodeposited ZnO thin films and nanowire arrays, respectively. The results show a typical nonlinear relationship revealing a Schottky contact between the ZnO nanowires and the bottom Au electrode. The difference (about one order of magnitude) of current value is due to the effective conductive section under the same electrode surface: the section sum of all nanowires connected to one microelectrode is smaller than the thin films' section which corresponds to the whole microelectrode surface.

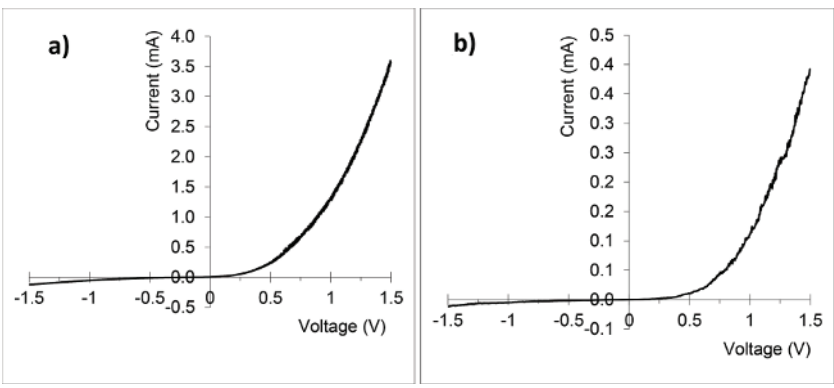

Figure 1.6. *Representative I–V characteristics under Al/ZnO/Au configuration from the ZnO thin film a) and nanowire arrays b), respectively, demonstrating typical Schottky contact behavior*

The classical expression of the *I–V* characteristics of Schottky contact cannot be directly adapted to fit the experimental data in this case due to the presence of series resistance R_s induced by the Au/ZnO interface. When the series resistance R_s is taken into account, the *I–V* characteristics can be represented as follows [SZE 81]:

$$I = I_s\left[(\exp(\frac{q(V\text{-}I\,R_s)}{nkT}) - 1\right] \qquad [1.1]$$

Figure 1.7(a) shows the forward *I–V* curve measured from the ZnO thin film, fitted with and without R_s using the systematic method proposed in the literature [CIB 85]. The series resistance R_s, the ideality factor n and the height of the Schottky barrier Φ_{sb} extracted from the fit with R_s are:

$$R_s = 108 \pm 15\ \Omega, \quad n = 10 \pm 1, \quad \text{and} \quad \Phi_{sb} = 0.39 \pm 0.01\ \text{eV}$$

Similarly, from the forward I–V curve obtained from the ZnO nanowire arrays, fitted with and without R_s (Figure 1.7(b)), we can obtain the corresponding series resistance R_s, the ideality factor n and the height of the Schottky barrier Φ_{sb}:

$$R_s = 783 \pm 60\ \Omega, \quad n = 10 \pm 1, \quad \text{and} \quad \Phi_{sb} = 0.36 \pm 0.02\ \text{eV}.$$

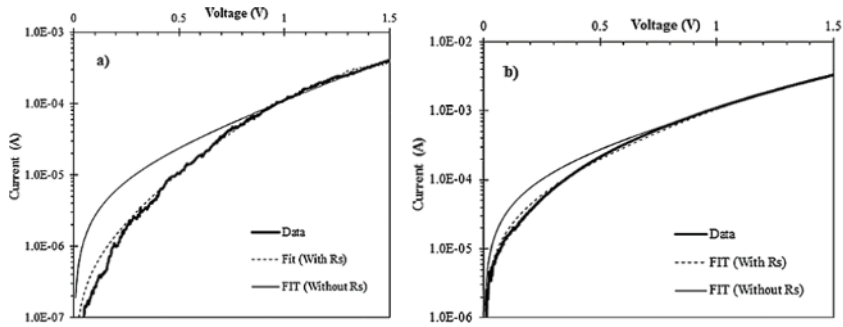

Figure 1.7. *I–V curves of ZnO thin films a) and ZnO nanowires b). Experimental data (bold line) compared to the fits without series resistance (solid line) and with series resistance (dashed line) according to Equation [1.1]*

Despite the inhomogeneity of the interface between the seed layer and the ZnO nanowires, we obtained the similar value of barrier height 0.39 and 0.36 for ZnO thin films and nanowires, respectively. These values are less than that reported on the Au/ZnO interface (summarized in Table 1.2 [OHA 02, POL 03, MEA 65, NEV 70, KOP 03, KLA 08]), which may be due to the trap of the charge carrier at the substrate during the first stage of the electrodeposition process. In fact, at the beginning of the ZnO growth, some charge carrier could be captured at the interface between Au substrate and the ZnO buffer layer. This will enhance the surface states which decrease the barrier height according to the Bardeen hypothesis [BAR 47].

ZnO synthesis method	*Au deposition method*	Φ_{SB} *(eV)*	*Measurement method*
Liquid phase epitaxy	Vacuum evaporation	0.50 [OHA 02]	*I–V*
CVT (bulk)	Vacuum evaporation	0.65 [POL 03]	*C–V*
Bulk	Thermal evaporation	0.71 [MEA 65]	Photo-response
CVD (bulk)	Thermal evaporation	0.66 [NEV 70]	*IV /C–V*
CVT (bulk)	Electron-beam	0.67 [KOP 03]	*I–V*
Aqueous chemistry (nanowires)	Thermal evaporation	0.70 [KLA 08]	*I–V*
Electrodeposition (thin film and nanowires)	Sputtering	0.39 and 0.36 [BRO 11]	*I–V*

Table 1.2. *Different Schottky barrier height values of the Au/ZnO junction obtained from different synthesis and measurement methods*

It is worth mentioning that the ideality factor n obtained from the electrodeposited ZnO thin films and nanowire arrays is ~10, higher than the unit value expected for an ideal diode. This indicates that electrical conduction mechanisms other than thermionic emission dominate the electronic transport through the electrodeposited ZnO/Au interface. Some mechanisms may become significant in such

nanostructural system, like the thermally activated tunnel effect, the tunnel effect assisted by structural defects and the recombination of electron-hole pairs.

Moreover, the high ideality factor value ~7.6 has also been observed on a Schottky junction between the ZnO nanowire (prepared by hydrothermal method) and the probing atomic force microscopy (AFM) tip coated with a gold layer. The authors attribute the high *n* value to the presence of the interface states between ZnO nanowire and the gold-coated tip [CHE 07].

In order to estimate the series resistance r_s of a single nanowire, the following assumptions can be made: all the nanowires are identical in length *l*, in diameter d, and have the same series resistance r_s. Under the above assumption, the nanowire arrays can be simplified to N parallel Schottky diodes, and the corresponding equivalent series resistance R_s of the nanowire arrays can be given by $R_s = \frac{r_s}{N}$, as shown in Figure 1.8.

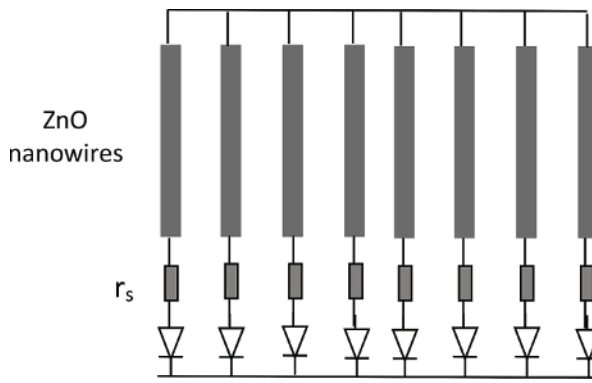

Figure 1.8. *Equivalent electrical circuits of the ZnO nanowire arrays*

The area of the top Al microelectrode on the nanowires is 6.4×10^3 μm^2 and the number of the nanowires contacted below the same microelectrode is estimated to be N ~38,400, obtained from the

nanowire density (~6 nanowires/μm^2, a statistical result from SEM plan view images). The series resistance r_s of a single ZnO nanowire is then given by $r_s = N R_s$. The numerical application with the values of $R_s = 783\ \Omega$ and N = 38,400 gives $r_s \approx 30\ M\Omega$.

This value is very important compared to the intrinsic resistance of a single nanowire which is estimated to be ~190 kΩ derived directly from the classical relation $R = \rho L/S$ with the values of $\rho = 0.06\ \Omega$ cm, L = 2.5 μm and $S = 7.85 \cdot 10^{-11}$ cm^2 (the cross-sectional area of the nanowire with 100 nm diameter).

However, we can also compare the series resistance obtained from the ZnO thin films with the nanowire arrays' resistance with the same electrical contact area: converting the electrode area on the ZnO thin film to equal contact area of N* nanowires of 100 nm in diameter. The full $6.4 \cdot 10^3$ μm^2 ZnO thin film can be considered as a system of N* parallel Schottky diodes, the number of the contact nanowires N* = 814,873. This leads to a nominal series resistance $Rs = 30\ M\Omega/N^* \approx 37\ \Omega$, which is the same order of magnitude as that obtained directly from the *I–V* measurement on the ZnO thin films ($Rs = 108\ \Omega$).

The difference can be explained by the proposed ideal model assuming a perfect homogeneity of the nanowires under same microelectrode, and in reality, all the nanowires do not participate effectively in the electrical measurements.

From the SEM images, it can be seen that some nanowires are tilted and there is a random distribution on the nanowire length. These observations remind us that the participation of the nanowires in the electrical measurement can be only partial. By comparing the experimental results obtained from two systems (nanowires and thin film), we suppose that almost one-third of nanowires are involved in the electrical measurement ($37/108 \approx 0.34$). Therefore, these results are very encouraging for the potential applications of ZnO nanowires such as electricity generation or solar cells, which require well-defined and reliable electrical contact with electrodes.

1.3. Optical properties of ZnO

ZnO is a transparent material in the visible range due to its wide gap, allowing it to be classified as a transparent conductive oxide (TCO).

Due to the anisotropy of its hexagonal crystal structure, the light propagating in a crystal ZnO will be subject to the optical birefringence phenomenon. The propagation of light in this case will take place in two directions: in the first direction, it will be propagated with a polarization parallel to the optical axis of the crystal (*c*-axis) and with a regular refractive index denoted as n_o; and in the second direction, it will be propagated with a polarization perpendicular to the optical axis and with an extraordinary refraction index denoted as n_e. Figure 1.9 shows the dispersion of the crystal ZnO refractive indices of the light as a function of wavelength.

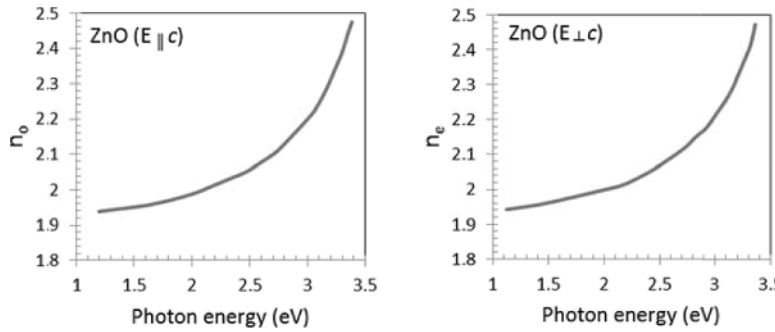

Figure 1.9. *Dispersion of the* regular *refractive index n_0 and the extraordinary refraction index n_e of the crystal ZnO*

The UV and photoluminescence emissions in ZnO nanocrystals have aroused great interest recently due to its UV and visible luminescence properties at room temperature in optoelectronic device applications [DJU 06, DJU 07, CHU 08]. The photoluminescence (PL) spectra of as-grown ZnO nanowires generally show a UV emission peak at ~384 nm with a dominant and broad emission in the visible region spanning from green to red (480 - 750 nm) (Figure 1.10(a)). The UV emission is well understood as near-band-

edge emission, while the origin of the visible emission, usually ascribed to the defect emission in the ZnO, is still not fully clear. Many controversial hypotheses have been proposed to explain the different origins, such as surface/shallow-level defects, e.g. oxygen vacancies and both oxygen and zinc interstitials [HEO 05], and surface hydroxides [XIE 06] as possible contributors.

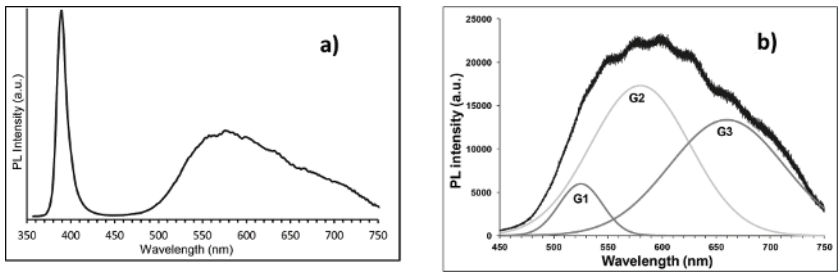

Figure 1.10. *PL spectrum of a hydrothermal-grown ZnO nanowire array a) and visible emission fitted by three Gaussians centered at ~525 (G1), ~580 (G2) and ~660 nm (G3), respectively b)*

In the literature, it has been proposed that the visible emission is made up of three main emissions in the green (515–530 nm), yellow-orange (570–600 nm) and red (660–680 nm), respectively, as shown in Figure 1.10(b). This hypothesis is quite well accepted by many research groups. The green luminescence is generally associated with oxygen vacancies [KWO 06], although this point remains controversial; whereas the yellow-orange emission has been assigned to interstitials oxygen [LI 04] and/or hydroxides groups [XIE 06, NOR 05, QIU 09] in the ZnO structure. The red emission has been reported to be associated with the oxygen excess [DJU 06, KWO 05]. These three emissions are usually attributed to oxygen vacancies, interstitials oxygen and/or hydroxides groups, and excess oxygen, respectively.

It is well known that the annealing treatment can improve crystalline quality and optical properties of ZnO nanowires [SUN 05, WIL 09]. Figure 1.11 shows the PL spectra of a hydrothermally grown ZnO nanowire sample before and after an annealing treatment at 400°C during 30 min in the air. Thus, the

emissions attributed to the vacancies (V_{Zn} and/or V_O), to the interstitial oxygen, and to the hydroxide groups were expected to evolve after annealing due to the ambient atmosphere of annealing operation. There is a reduction of the visible emission. In fact, the defects induced in the ZnO nanostructural sample during the synthesis process, for example, due to the solution concentration variation, can be reduced via the annealing treatment. The post-annealing reduces mainly the green emission, resulted from the oxygen vacancy defect, and the other defect diminution is less significant. Furthermore, an overall red-shift of the visible emission can be observed in the annealed sample PL spectra compared to the as-grown ones. This phenomenon is also observed by Djurišić *et al.* [DJU 07] for all annealed samples compared to the as-grown ones.

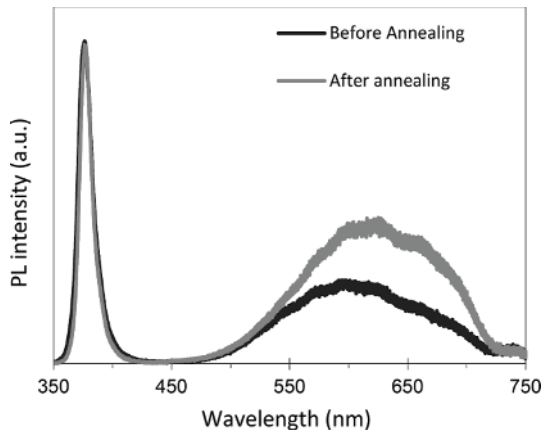

Figure 1.11. *PL spectra of a hydrothermal-grown ZnO nanowire sample before and after an annealing treatment at 400°C during 30 min in the air*

1.4. Piezoelectricity of ZnO

In single crystal piezoelectric solids, the piezoelectric property of the material originates in its atoms and is repeated throughout the solid due to high crystallinity. The non-symmetric distribution of positive and negative charges starts from a unit cell and repeats through the whole material; thus, a strained material results in a net polarization on the surface.

ZnO belongs to the class of piezoelectric materials and its anisotropic piezoelectric properties are due to its crystal structure which belongs to $P6_3mc$ symmetry group having no center of symmetry [KON 03]. In this case, the unit cell barycenters of positive and negative charges do not overlap. Thus, an electric dipole appears within the crystal and it can be modulated by the application of mechanical stress (direct piezoelectric effect), as shown in Figure 1.12. The interaction of the electric dipole with an external electric field can also deform the crystal (inverse piezoelectric effect).

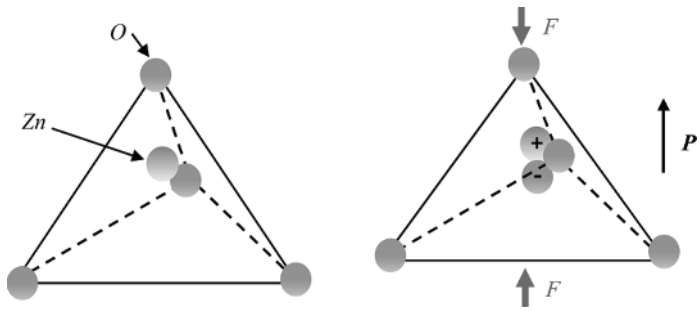

Figure 1.12. *Piezoelectric effect in ZnO unit cell (P – dipole vector)*

The concept of piezoelectricity is based on the coupling between the mechanical properties and electrical properties of the material. These two properties are related to each other through the tensors. Strongly, the mechanical and electrical behavior of a piezoelectric material can be modeled by two linearized constitutive equations. These equations contain two mechanical and two electrical variables. The direct piezoelectric effect and the converse piezoelectric effect may be modeled, respectively, by two following constitutive matrix equations:

$$\boldsymbol{D} = d \cdot \boldsymbol{T} + \varepsilon^T \cdot \boldsymbol{E} \qquad [1.2]$$

$$\boldsymbol{S} = s^E \cdot \boldsymbol{T} + d^t \cdot \boldsymbol{E} \qquad [1.3]$$

where $\boldsymbol{D}$ is the electric displacement vector, $\boldsymbol{T}$ is the applied mechanical stress vector, ε^T is the dielectric permittivity matrix at

constant mechanical, ***E*** is the electric field vector, ***S*** is the mechanical strain vector, s^E is the matrix of elasticity under conditions of constant electric field, and d and d^t are the piezoelectric charge coefficients, respectively, for the direct piezoelectric effect ($C \cdot N^{-1}$) and the converse piezoelectric effect ($m \cdot V^{-1}$), where *t* denotes the transposed matrix. The piezoelectric coefficients of the direct piezoelectric effect (d) and the converse piezoelectric effect (d^t) are thermodynamically identical, i.e. $d_{direct} = d_{converse}$. Note that the sign of the piezoelectric charge ***D*** and strain ***T*** depends on the direction of the mechanical and electric fields, respectively, and the piezoelectric coefficient d can be either positive or negative.

The piezoelectric coefficient d_{ij} is the ratio of the strain in the j-axis to the electric field applied along the i-axis, when all external stresses are held constant. The piezoelectric constant d_{31} is usually a negative number. This is due to the fact that the application of a positive electric field will generate a positive strain in direction 3.

There are two practical coupling modes in the piezoelectric material: the stack configuration operating in the 33 mode and the bend configuration operating in the 31 mode as shown in Figure 1.13. The sign convention assumes that the poling direction is always in the "3" direction.

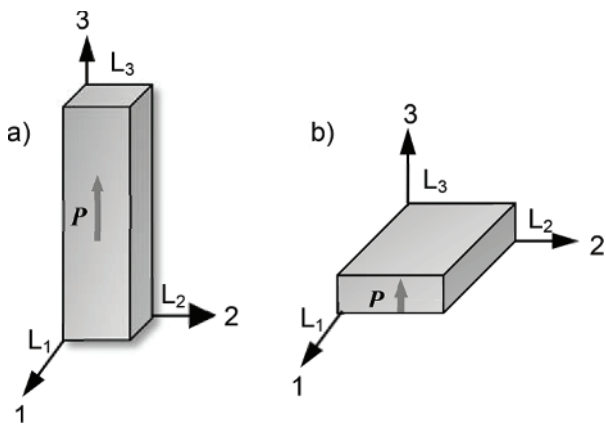

Figure 1.13. *Illustration of two operating modes for the piezoelectric material: a) 33 mode and b) 31 mode*

For the force applied in the direction perpendicular to the poling direction, such as bending, d_{31} will be applied; and for the force applied in the same direction as the poling direction, such as the compression, d_{33} will be applied. In 31 mode, the electric field is along the polarization axis (direction 3), but the strain is in the 1 axis (orthogonal to the polarization axis). In 33 mode, the electric field is along the polarization axis (direction 3) and the strain (deflection) is along the same axis. Conventionally, the 31 mode has been the most commonly used coupling mode in the energy harvesting via piezoelectric effect, but the piezoelectric coefficient d_{31} is lower than d_{33}.

The ZnO crystal is anisotropic; its piezoelectric coefficients are different depending on its orientation. d_{33} = 12.4 pm/V is the accepted piezoelectric coefficient of single crystal ZnO [CHR 98], $d_{31} = -5.1$ pm/V is also reported [BER 97].

It was found that the 31 configuration cantilever proved to be the most efficient under small force and in low vibration-level environment; on the other hand, in large force and high frequency environment, the 33 configuration cantilever would be more efficient to generate energy. It was also found that the resonant frequency of a system operating in the 31 mode is much lower than the system operating in the 33 mode. So, the system in 31 mode is more likely to be driven at resonance in a natural environment, thus providing more power.

ZnO nanowires are more flexible than bulk materials due to their high aspect ratio (length/diameter), thus, under the same mechanical strain, the high aspect ratio nanowires can withstand larger amounts of strain to provide more mechanical energy available for conversion into electrical energy. This is why ZnO nanowires become a very promising piezoelectric material for energy harvesting.